Interfacial bond strength of electrophoretically deposited hydroxyapatite coatings on metals

M. WEI*, A. J. RUYS†, M. V. SWAIN‡, S. H. KIM*, B. K. MILTHORPE§, C. C. SORRELL*

**School of Materials Science and Engineering, University of New South Wales, Sydney, NSW 2052, Australia*

‡*Biomaterials Science Unit, University of Sydney, Sydney, New South Wales 2052, Australia*

†*Centre for Advanced Materials Technology, Department of Mechanical & Mechatronic Engineering, University of Sydney, NSW 2006, Australia*

§*Graduate School for Biomedical Engineering, University of NSW, Sydney, NSW 2052, Australia*

Hydroxyapatite (HAp) coatings were deposited onto substrates of metal biomaterials (Ti, Ti6Al4V, and 316L stainless steel) by electrophoretic deposition (EPD). Only ultra-high surface area HAp powder, prepared by the metathesis method ($10Ca(NO_3)_2 + 6(NH_4)_2HPO_4 + 8NH_4OH$), could produce dense coatings when sintered at 875–1000 °C. Single EPD coatings cracked during sintering owing to the 15–18% sintering shrinkage, but the HAp did not decompose. The use of dual coatings (coat, sinter, coat, sinter) resolved the cracking problem. Scanning electron microscopy/energy dispersive spectroscopy (SEM/EDS) inspection revealed that the second coating filled in the ''valleys'' in the cracks of the first coating. The interfacial shear strength of the dual coatings was found, by ASTM F1044-87, to be $\sim$ 12 MPa on a titanium substrate and $\sim$ 22 MPa on 316L stainless steel, comparing quite favorably with the 34 MPa benchmark (the shear strength of bovine cortical bone was found to be 34 MPa). Stainless steel gave the better result since α-316L (20.5 $\mu m\, mK^{-1}$) > α-HAp ($\sim$ 14 $\mu m\, mK^{-1}$), resulting in residual compressive stresses in the coating, whereas α-titanium ($\sim$ 10.3 $\mu m\, mK^{-1}$) < α-HAp, resulting in residual tensile stresses in the coating.

1. Introduction

1.1. Hydroxyapatite coatings

Deposition of bioactive coatings of hydroxyapatite (HAp) onto the surface of metal implants is a relatively recent development in clinical orthopaedics [1]. These bioactive surface films are typically tens of micrometers thick. Thermal spraying [2] is the most developed process for depositing these HAp coatings and thermally sprayed implants have been used in clinical practice for some years now. Thermal spraying is a costly procedure and it is a line-of-sight process and is therefore not always ideal for coating implants of complex shape or morphology (mesh, macropores, etc.). However, thermal spraying has been the method of choice because with thermal spraying, deposition and densification of the HAp coatings occur simultaneously, whereas most of the other coating methods require a subsequent densification stage that involves heating the coated implant to sinter the HAp coating. The sintering temperature of HAp is generally above 1150 °C.

1.2. Electrophoretic deposition

Electrophoretic deposition (EPD) [3] is a low-cost flexible coating process, and, being a non-line-of-sight coating process, it can be used to deposit even coatings on substrates of complex shape or surface morphology. Furthermore, EPD can produce coatings of a wide range of thicknesses, from < 1 μm to > 100 μm, with a high degree of control over coating thickness and morphology. As for many other ceramic coating techniques, EPD-coated implants need a subsequent densification stage in order to sinter the coating. This requirement poses something of a dilemma. If the thermal expansion coefficient (α) of the ceramic coating is lower than for the substrate, then the coating is placed in compression on cooling, and if higher, then the coating is placed in tension on cooling. Ideally, the thermal expansion coefficient of the coating and substrate should be very similar with α-coating slightly lower than α-substrate, since this will result in weak compressive residual stresses in the coating, which will inhibit cracking.

‡Corresponding author: Dr Andrew J. Ruys. Email: a.ruys@mech.eng.usyd.edu.au.

A further issue is the deleterious effects of temperature on the properties of the coating and the metal substrate. Low sintering temperatures can lead to weakly bonded low-density coatings. High sintering temperatures can result in degradation of the metal substrate (oxidation and impaired mechanical properties) and also degradation of the HAp as a result of the metal substrate catalyzing decomposition of the HAp to anhydrous calcium phosphates [4, 5]. Decomposition is undesirable as it leads to enhanced *in vitro* dissolution rates [6]. Pure HAp decomposes in the temperature range 1250–1450 °C [7]. Previous studies have demonstrated that the presence of fibers or particles in a HAp matrix reduces its decomposition temperature from the usual range of ∼ 1300–1400 °C (pure HAp) down to ∼ 750–1150 °C [4, 5, 8]; titanium induces decomposition above ∼ 1050 °C [5] and 316L stainless steel induces decomposition above ∼ 950 °C [4]. A high sintering temperature is also problematic for the metal substrate because it can lead to phase transformation and grain growth. This may cause the mechanical properties of the metal substrate to decrease significantly. A recent study by the authors has demonstrated that the mechanical properties of these titanium alloys and 316L stainless steel degrade significantly when heated above 1050 °C [9]. Therefore, to minimize degradation of the HAp and of the metal, densification temperatures ideally should be below 1000 °C if possible. Densification of HAp follows a sigmoidal correlation with the following two characteristic parameters [7]:

Plateau temperature : calcined HAp 1150 – 1300 °C;
raw uncalcined HAp < 1050 °C

Plateau density : calcined HAp 80 – 95%;
raw uncalcined HAp > 98%

Therefore, to reduce the HAp densification temperature to such low temperatures, ultra-high surface area HAp powders need to be used, which generally means uncalcined HAp. Until recently, it was believed that uncalcined HAp powders could not be deposited onto metallic substrates by electrophoresis. However, recent work by the present authors indicated that uncalcined HAp powders could be deposited by electrophoresis, and that dense and even HAp coatings could be produced [10]. This finding was confirmed by the successful deposition of uncalcined metathesis HAp onto metallic substrates by Zhitomirsky and Gal-Or in 1997 [11].

Therefore, the present EPD study focused on uncalcined HAp powders, utilizing both a commercial powder and a powder produced in-house by the metathesis process [12]. The metathesis process involves the precipitation of calcium phosphate and subsequent alkali digestion in aqueous ammonia at a pH of 11–12, according to the following chemical reaction

$$10Ca(NO_3)_2 + 6(NH_4)_2HPO_4 + 8NH_4OH \Rightarrow$$
$$Ca_{10}(PO_4)_6(OH)_2 + 20NH_4NO_3 + 6H_2O$$

1.3. Interfacial bond strength

The HAp coating provides a bioactive surface on a metal implant for bone ongrowth. Therefore, it is important that the coating–implant interfacial bond strength is sufficiently high to withstand the interfacial stresses encountered in the *in vivo* environment. No standardized test has yet been developed for determining the fracture resistance and adhesive bonding strength of ceramic coatings [13]. All testing methods are limited to some envelope of material properties and testing conditions [14]. Tensile and shear strength tests are the main procedures used for quantifying the adhesion of HAp on metal substrates. This is mainly because of their simplicity and the existence of the test standards [15–20]. The available standards are: ASTM C633 and F1147 for tensile strength testing [18, 19] and ASTM D4501 and F1044 for shear strength testing [17, 20]. In addition, there are some other variations of tensile testing methods, such as indentation, scratching, hammering, metal stamping, coining, and rolling with slip, all of which have been used for different coating techniques [21, 22]. In particular, macroindentation and microindentation have been extensively used to assess hard thin films [14, 23].

1.4. The shear strength test

This test relies on a bonding agent to remove the film with an applied shear strength [24], as shown in Fig. 1. It is a simple testing method and there is an existing standard to follow [20]. Further, the data analysis of this test method is simple and the strength can be easily calculated from the fractured force over the fracture area. However, as a bonding agent is required in this test, it is possible that the bonding agent (for example, epoxy resin) may penetrate through macropores or cracks in the film and partially bond to the substrate, thereby compromising the validity of the test result. Therefore, careful attention must be paid to the issue of adhesive penetration. Such issues were a principal focus of the present study.

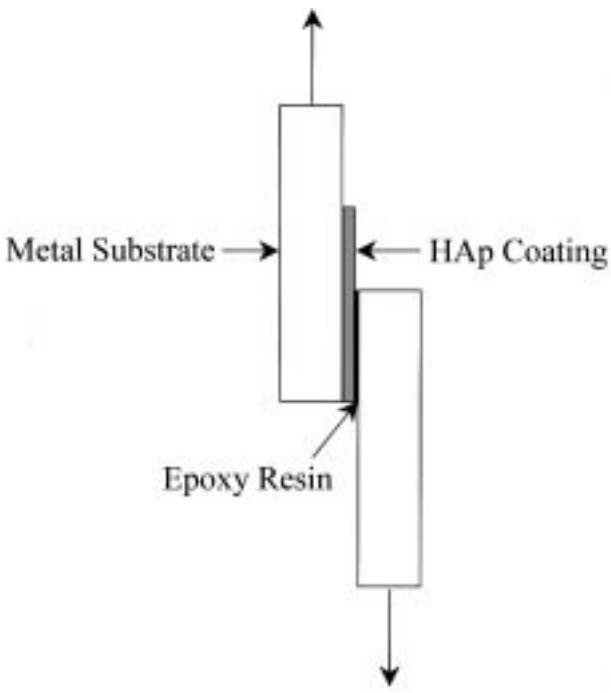

Figure 1 The coating shear-strength testing procedure, from ASTM F1044.

2. Experimental procedure

2.1. Hydroxyapatite powders

Two ultra-high surface area HAp powders were used:

1. A commercially available product (Merck, Germany) designated Merck HAp. Various commercially available HAp powders were tested by the BET method (Phlosorb, UNSW), and the Merck powder was found to have the highest surface area, and this was the reason for its selection.

2. An uncalcined powder, produced in-house by the metathesis method [12], designated metathesis HAp. It was produced using 99.0% pure $Ca(NO_3)_2 4H_2O$ (Ajax Chemicals) and 98% pure $(NH_4)_2HPO_4$ (Ajax Chemicals). After precipitation, the resulting metathesis HAp suspension was aged in its mother liquor at room temperature for 100 days by vigorous stirring using a magnetic stirrer.

2.2. Dilatometry

The metal substrates used were Ti, Ti6A14V, and 316L, because these are the principal metals used to fabricate commercially available metal implants. The thermal expansion coefficients of each of these three metals and the two HAp powders were evaluated by dilatometry (Orton Model 1600). Pelletized HAp specimens (diameter 13 mm, length 20–25 mm) were prepared by uniaxial pressing at 50 MPa. Metal specimens were cut to size. The measurements were carried out separately for all samples. The two HAp samples were tested in air and the metal samples were tested in argon. All the samples were heated to 1000 °C at a heating rate of 100 °C h^{-1} and then cooled to 200 °C at a rate of 50 °C h^{-1}. The thermal expansion coefficients were calculated from the cooling curves, and the shrinkage of the ceramic specimens during heating (densification) was also noted.

2.3. Electrophoretic deposition

Specimens were prepared from each of the three coating substrates (Ti, Ti6A14V, and 316L stainless steel). They were cut into samples of the shape shown in Fig. 2. before deposition, the substrates were sandblasted with commercial garnet (Sandblasting and Metallizing Service Pty Ltd, Australia) and its surface roughness was measured using a fine probe at a number of locations and the arithmetic mean determined (alpha-step 200, Tencor Instruments). Before deposition, the sandblasted substrates were thoroughly washed with a commercial detergent (Diversey, pyrogenically negative cleaner) in an ultrasonic bath for ~ 30 min, followed by washing in acetone (95.9%, Ajax Chemicals) for another 15 min, then passivated in 25 vol% nitric acid (69.0–71.0%, Ajax Chemicals) overnight. Deposition suspensions of metathesis HAp and Merck HAp were then prepared by mixing 0.5 g HAp in 100 ml of ethanol. Ethanol was used because recent experimentation by the authors had demonstrated its suitability to the role. The ethanol suspensions were sonified in an ultrasonic bath for 0.5 h before deposition. During deposition, the substrate acted as the cathode and a parallel 20 × 35 mm copper plate was used as the anode. The deposition voltage was 50 V and the deposition time was 5 min and 2 min for metathesis HAp and Merck HAp, respectively, to compensate for their different deposition rates. The coated samples were then slowly dried in a sealed dessicator so as to minimize the risk of cracking during drying. It took ~ 5 h for the samples to dry completely.

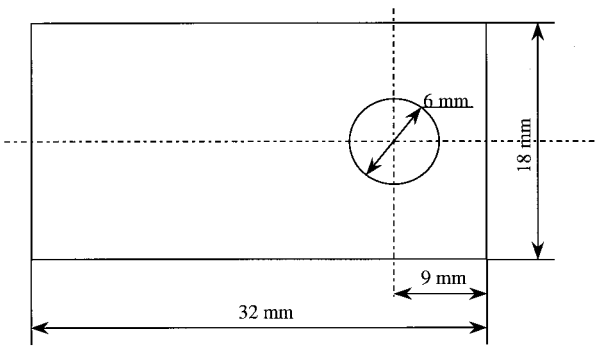

Figure 2 The shape and dimensions of the specimens used in the coating shear-strength test.

2.4. Densification

The coated samples were sintered in a resistance tube furnace under flowing high-purity argon gas. All the samples were supported on HAp granules during sintering. The sintering temperature was in the range 875–1000 °C at intervals of 25 °C. The heating rate was 100 °C h^{-1}, the soak time was 1 h, and the cooling rate was 50 °C h^{-1}. A second coating was then applied by EPD using the same HAp powder and deposition parameters as for the first layer, and the drying and sintering processes were repeated. After sintering, the second coating was analyzed by X-ray diffraction (Siemens D5000) to determine whether decomposition of the HAp had occurred during densification.

After the second coating layer was densified, morphological assessment of the coated specimens was conducted by scanning electron microscopy (SEM: Cambridge Stereoscan S360). The specimens were adhered to an aluminum stub using silver paste, then gold-coated (Coating Unit E5000, Polaron Equipment Limited). SEM examination was carried out using an accelerating voltage of 20 kV and a magnification of 500 ×.

2.5. Shear strength measurement

A group of 316L stainless steel specimens were cut into the same shape as the coated metal specimens (Fig. 2), and these were used as the counter-members in the shear-test configuration, as shown in Fig. 1. These counter-member pieces were thoroughly washed in detergent, acetone, and nitric acid, using the same procedure used for the substrates for coating (the process described in Section 2.3.). Before testing, the coated samples were glued to the washed 316L strips with epoxy cement (Araldite, Selleys Chemical Company) and then oven-cured at 100 °C for approximately 2 h.

The adhesive strength of the coating was tested according to ASTM F1044-87 [20]. Testing was carried

out with a universal testing machine (Model 4302, Instron Ltd) using a 10 kN load cell and a crosshead speed of 1.0 mm min^{-1}, with the configuration shown in Fig. 1. The testing rig was fabricated from 316L stainless steel. The peak force was recorded and the fracture area was measured by dial callipers. The adhesive strength was calculated as the peak force/fracture area. Five samples in each group were tested and the average value was used as the final result.

The shear-fracture surfaces of the coated specimens were then assessed by SEM and energy dispersive spectroscopy (EDS: Kevex delta plus EDS analyzer, Kevex Instruments). EDS was used to detect the composition of the fracture surface, specifically to detect the presence of HAp, metal oxide, and epoxy resin, thereby determining the nature of the failure, whether HAp–oxide or HAp–HAp, and to detect whether or not epoxy resin penetrated to the fracture surface. The presence of epoxy resin at the fracture surface would indicate that the measured interfacial stress of that specimen was a false result.

The shear strength of cortical bone was measured in order to give a point of comparison for the coating–metal shear strength measurements. The test was based on ASTM D 4501-95 [17]. A section of bovine iliac crest cortical bone was cut into ten samples of approximate size 4 × 8 × 20 mm. The shear strength test was carried out on the Instron testing machine with a 10 kN load cell and a crosshead speed of 100 mm min^{-1}. The test is illustrated in Fig. 3. The fracture force was recorded for each specimen, and the length and width of the fractured area were measured using callipers, to give the shear strength (fracture force/fracture area). The average value of 11 specimens was used as the final result.

3. Results and discussion

3.1. Dilatometry

The dilatometry plots for each of the three metals and the two HAp powders are shown in Fig. 4. From this figure, the thermal expansion coefficient (α) of Ti, Ti6Al4V, 316L stainless steel, and HAp, were derived. These data are compiled in Table I revealing that α-316L was $\sim$ 45% greater than α-HAp, while α-Ti and α-Ti6Al4V were both $\sim$ 25% lower than α-HAp. The shrinkage data for the Merck HAp and the metathesis HAp revealed the following:

3.1.1. Merck HAp

Although this had the highest surface area of the commercial powders tested, only a minor amount of densification occurred by 1000 °C ($\sim$ 7% linear shrinkage). This demonstrated the necessity of using raw uncalcined HAp when such low densification temperatures are involved.

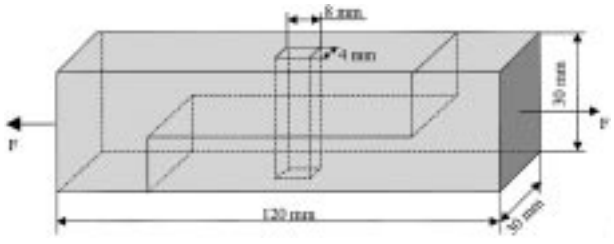

Figure 3 The procedure used for testing the shear strength of the cortical bone specimens, from ASTM D4501.

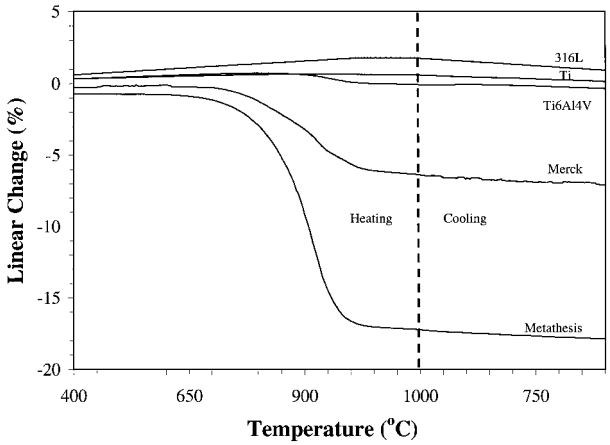

Figure 4 Dilatometry plots for the three metals (Ti, Ti6Al4V, and 316L stainless steel) and the two HAp powders (Merck HAp, and metathesis HAp).

3.1.2. Metathesis HAp

This raw uncalcined HAp was almost fully densified by 1000 °C ($\sim$ 18% linear shrinkage). Shrinkage for a fired ceramic is typically 15 to 20%, and so this metathesis HAp coating was approaching full densification at 1000 °C.

3.2. Densification

The surface morphologies of the metathesis HAp coatings on Ti, Ti6Al4V, and 316L stainless steel are shown in Figs 5, 6, and 7, respectively. These figures reveal a ''dried mud'' type cracking configuration that is indicative of high shrinkage. High shrinkage was to be expected because the data from Fig. 4 reveal that when fired to 925 °C, metathesis HAp underwent $\sim$ 15% linear firing shrinkage, and was therefore near fully dense. X-ray diffraction analysis revealed that the second coating after densification contained no anhydrous calcium phosphate phases, only HAp.

The surface morphologies of the Merck HAp coatings on Ti, Ti6Al4V, and 316L stainless steel are shown in Figs 8, 9, and 10, respectively, revealing that no cracking occurred. The data from Fig. 4 reveal that Merck HAp

TABLE I Dilatometry data: thermal expansion coefficients; total linear shrinkage for the HAp after heating to 1000 °C

Material	Thermal expansion coefficient ($\mu m\, mK^{-1}$)	Total linear shrinkage (%)
Ti	10.4	–
Ti6Al4V	10.3	–
316L	20.5	–
Merck HAp	14.6	7.09
metathesis HAp	13.4	17.87

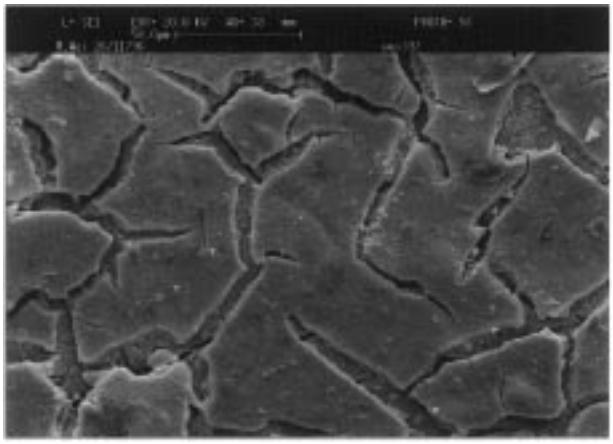

Figure 5 Surface morphology by SEM of metathesis-HAp-coated Ti.

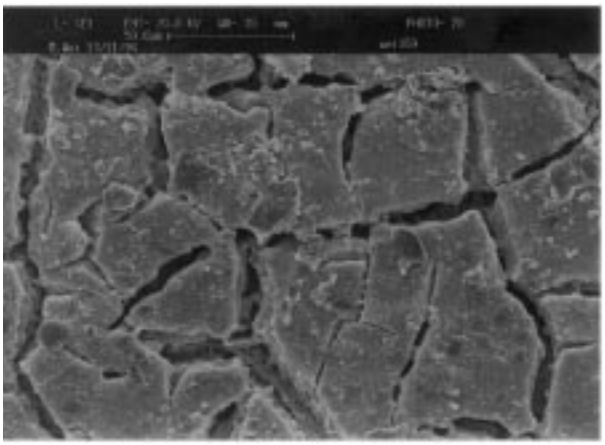

Figure 7 Surface morphology by SEM of metathesis-HAp-coated 316L stainless steel.

underwent less than 5% firing shrinkage when fired to 925 °C. Furthermore, the fired coatings had negligible adhesive strength and could be easily scraped off. Therefore, the lack of cracking was merely indicative of the fact that the coating had undergone negligible densification at 925 °C. Therefore, two important conclusions can be drawn from these densification findings:

1. Inadequate densification leads to inadequate adhesive strength.
2. Adequate densification, and the associated high degree of shrinkage, lead to cracking because the shrinkage of the dense coating causes tensile stresses and hence cracking.

These problems were overcome by depositing double coatings of the metathesis HAp. This HAp densified significantly at temperatures < 1000 °C. The measured shear strengths of the double layer metathesis HAp coatings proved the effectiveness of this approach.

3.3. Shear strength

The bonding strength of the Merck HAp coatings, densified at 1000 °C or below, was insignificant owing to inadequate densification. Therefore, the shear strength measurements were meaningful for metathesis HAp coatings only. Although SEM showed that the metathesis HAp coatings were significantly cracked, EDS analysis of the fracture surface of shear-tested metathesis HAp-coated specimens showed that for almost all specimens, there was no penetration of the epoxy resin to the fracture interface. The fracture surface of the majority of the test specimens comprised metal oxide, as shown in Fig. 11. A metal oxide fracture surface infers that fracture occurred at or below the interface between the HAp coating and the oxidized surface of the metal, in which case the measured shear strength was representative of the coating–substrate interfacial bond.

A few specimens fractured within the HAp coating itself, and such fracture surfaces contained a mixture of epoxy resin and HAp, as shown in Fig. 12. Such specimens were atypical and the ''shear-strength'' results from these specimens were not valid. The difference between these unrepresentative specimens and the representative specimens are shown in the schematic of a coating cross-section in Fig. 13.

Therefore, the fact that the majority of specimens fractured at the HAp/metal-oxide interface, and the fact that epoxy penetration did not extend to this interface, suggests that the ''dual coating'' strategy was successful in overcoming the problem of loss of interfacial strength through ''dry mud'' cracks forming during densification. The probable explanation for the success of the dual coating strategy was as follows:

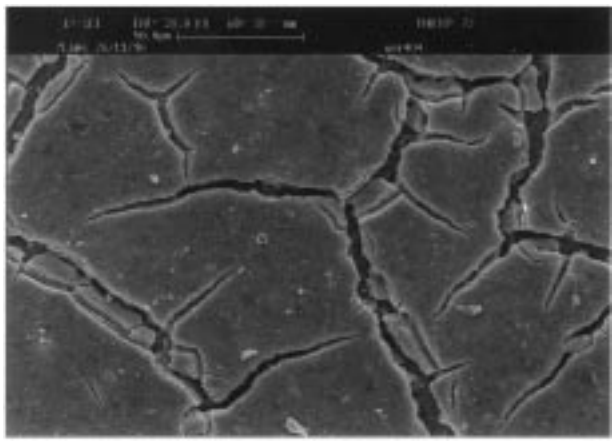

Figure 6 Surface morphology by SEM of metathesis-HAp-coated Ti6Al4V.

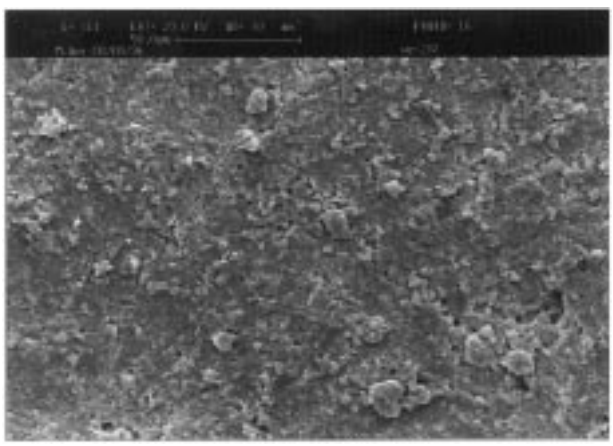

Figure 8 Surface morphology by SEM of Merck-HAp-coated Ti.

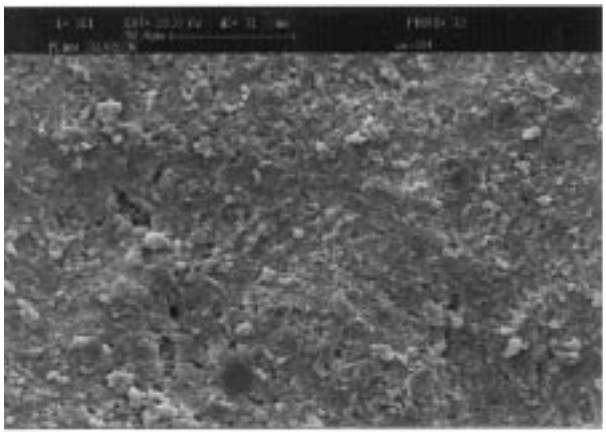

Figure 9 Surface morphology by SEM of Merck-HAp-coated Ti6Al4V.

- Coating 1 cracked extensively during the shrinkage associated with densification.
- When coating 2 was deposited, it filled in the ''valleys'' (deep regions) of the ''coating 1 cracks''.
- During densification of coating 2, coating 2 cracked at the upper surface.
- During densification of coating 2, the crack-filling of the ''valleys'' in the ''coating 1 cracks'' resulted in crack-healing of coating 1.

Cross-sectional SEM micrographs of metathesis HAp coatings on Ti, Ti6Al4V, and 316L stainless steel substrates are shown in Figs 14, 15, and 16, respectively. The Ti6Al4V specimen in particular shows evidence of ''valley filling''. While the coatings and the metal substrates appear to be near fully dense, the oxide–HAp interfacial region is clearly seen to be a zone of weakness, containing significant microporosity. This accords with the finding that, in most specimens, shear failure occurred at the oxide–HAp interface.

This dual coating approach resulted in a moderate interfacial strength, as shown in the plots of shear strength versus densification temperature for Ti, Ti6Al4V, and 316L substrates (Figs 17, 18 and 19, respectively). The shear strength appeared to be independent of temperature within the 875–1000 °C range, as the results seem to indicate random scatter about a mean value. The possible exceptions were

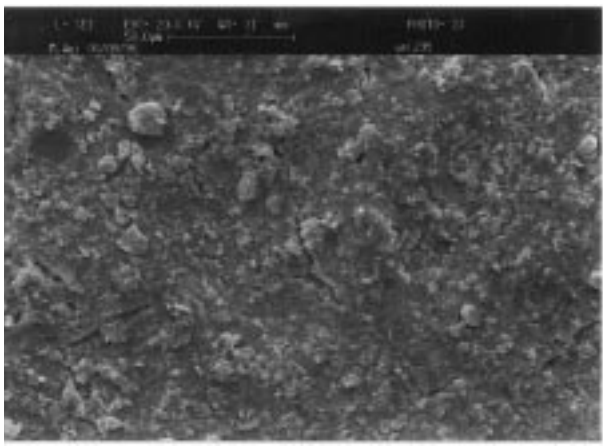

Figure 10 Surface morphology by SEM of Merck-HAp-coated 316L stainless steel.

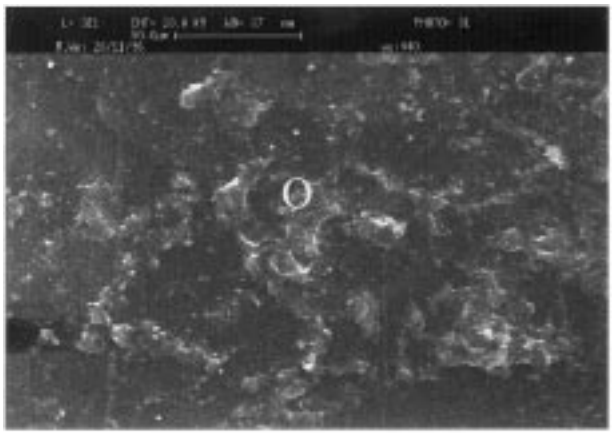

Figure 11 SEM fracture surface morphology of a metathesis-HAp-coating after a successful shear-strength test (EDS confirmed that the surface comprised only metal oxide).

stainless steel below 900 °C and titanium above 950 °C, but the size of the error bars suggests that these apparent trends were probably not significant, rather they were probably artifactual.

From these figures, this mean value, the average shear strength, was calculated for each substrate (s = standard deviation).

$$\text{Ti: } 13.9 \text{ MPa } (s = 4.3)$$
$$\text{Ti6Al4V: } 11.0 \text{ MPa } (s = 7.8)$$
$$\text{316L: } 22.4 \text{ MPa } (s = 3.6)$$

As expected, Ti and Ti6Al4V were similar. In comparison, stainless steel had a much higher shear strength and much less scatter in strength as reflected in the standard deviations and their proportion of the mean, as well as by larger degree of scatter in Figs 17 and 18 (Ti and Ti6Al4V) compared with Fig. 19 (stainless steel). As the dilatometry data showed, α-stainless steel was $\sim 45\%$ higher than α-HAp, and therefore on cooling after densification, the stainless steel substrate would have placed the coating in significant compression, thereby inhibiting cracking. In contrast, α-Ti and α-Ti6Al4V were $\sim 25\%$ lower than α-HAp, and therefore, these titanium substrates would have placed the coating in tension during cooling, thus exacerbating cracking. This is demonstrated in the coating cross-

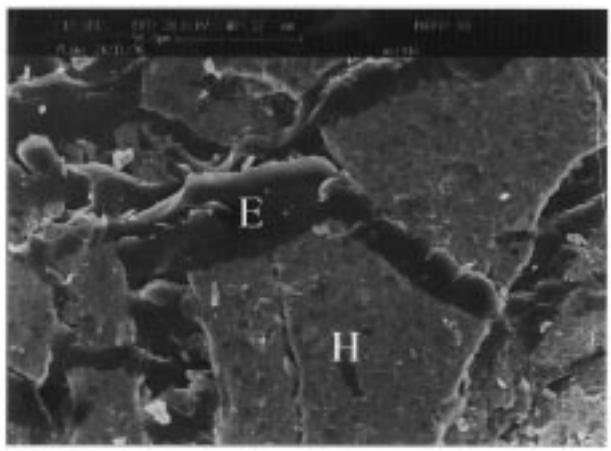

Figure 12 SEM fracture surface morphology of a metathesis HAp-coating after an unsuccessful shear strength test (EDS comfirmed that the surface contained regions of HAp and epoxy resin).

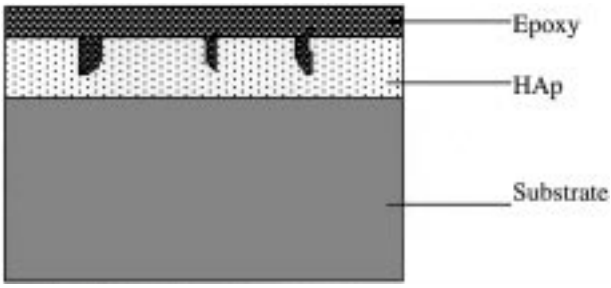

Figure 13 Schematic of the coating cross-section of test specimens. The specimens with no epoxy on the fracture surface fractured at the HAp-substrate interface. The specimens with HAp and epoxy on the fracture surface fractured within the coating, through the HAp and the epoxy regions above the interface.

sectional micrographs (Figs 14–16). Both the Ti and the Ti6Al4V specimens show evidence of fine cracks due to thermal expansion mismatch, while the 316L specimen shows no such fine cracks.

The shear strength measurements of the bovine cortical bone yielded an average shear strength of 34 MPa with a standard deviation of 17 MPa, indicating significant variation between the 11 bone specimens tested. Significantly, the interfacial bond strength of thermally sprayed HAp is around 35 MPa, with a significant scatter about this average [25]. Therefore, 34 MPa appears to be a representative benchmark figure for HAp coating shear strength. The interfacial bond strengths determined for the EPD HAp dual-coatings of this investigation were between 30 and 40% of the benchmark for titanium/titanium alloy, and $\sim$ 65% of the benchmark for stainless steel. The reasons for this difference are probably as follows:

3.3.1. Titanium/titanium alloy 30–40% of benchmark strength

The residual stress is tensile. This creates a tendency for cracking. This was reflected in the coating cross-sections (Figs 14 and 15) and in the lower interfacial strength than for stainless steel.

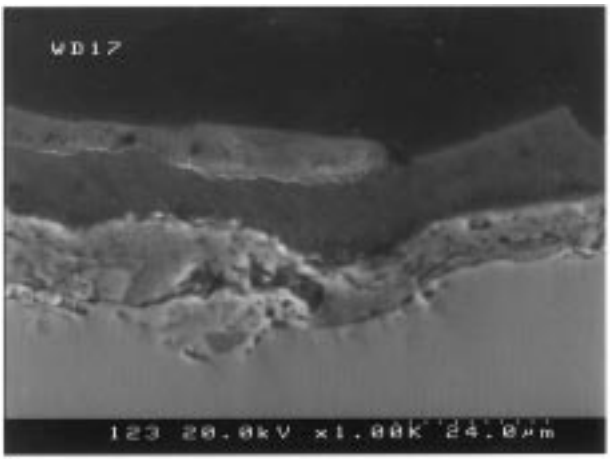

Figure 14 SEM cross-sectional micrograph of a HAp-Ti coating. Note evidence of fine cracks due to thermal expansion mismatch.

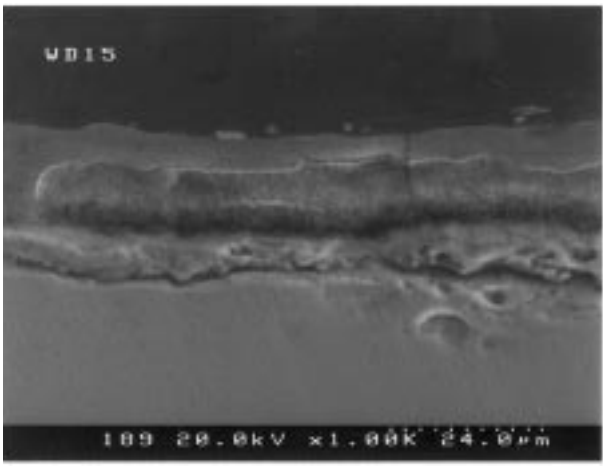

Figure 15 SEM cross-sectional micrograph of a HAp-Ti6Al4V coating. Note evidence of ''valley filling'' by coating 2 in the macrocrack of coating 1 (left hand end of the interface) and some fine cracks due to thermal expansion mismatch.

3.3.2. Stainless steel 65% of benchmark strength

The residual strength was compressive. This created a tendency for buckling-driven film delamination. While this mechanism degraded the interfacial strength, the degradation was not as severe as for the residual-tensile scenario of titanium, as reflected in the superior interfacial strength and in the absence of fine cracks in the micrograph in Fig. 16. While $\sim$ 22 MPa falls short of the interfacial strength of thermally sprayed coatings, it is still a positive outcome in light of the fact that EPD has a low processing cost and is a non-line-of-sight process.

4. Conclusions

1. EPD coatings of ultra-high surface area HAp onto metal substrates resulted in significant cracking during densification owing to the 15–18% shrinkage associated with densification of the ceramic coating.

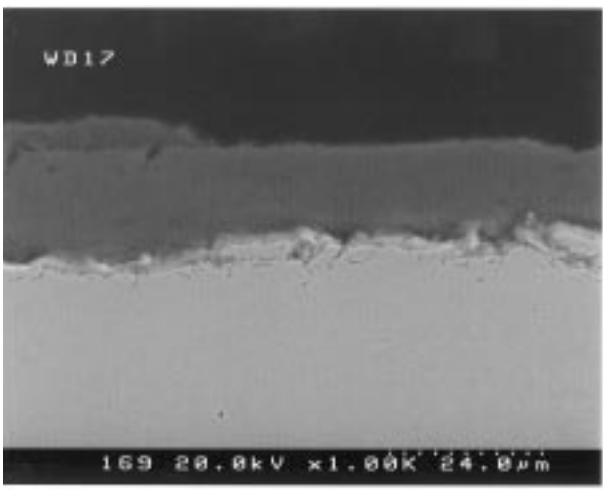

Figure 16 SEM cross-sectional micrograph of a HAp-stainless steel coating. Note the absence of fine cracks owing to residual compressive stresses.

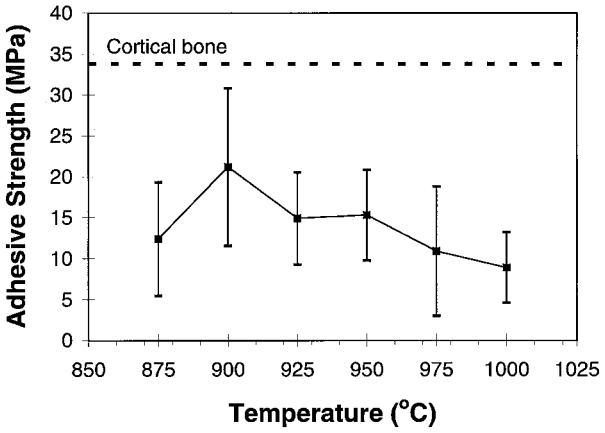

Figure 17 Interfacial shear strength, as a function of densification temperature, for a Ti substrate.

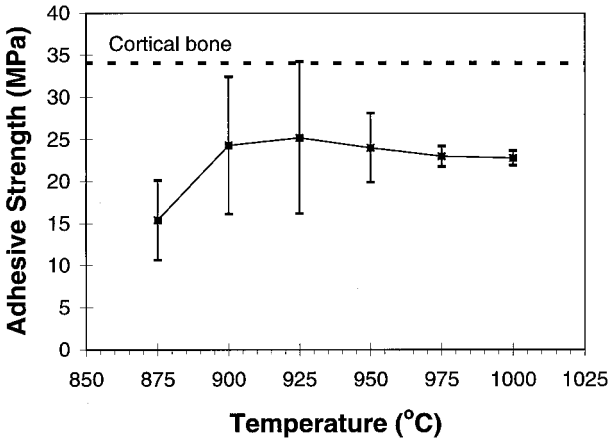

Figure 19 Interfacial shear strength, as a function of densification temperature, for a 316L stainless steel substrate.

2. The use of dual coatings (coat, sinter, coat, sinter) resolved this problem. The second coating filled in the ''valleys'' in the cracks of the first coating.

3. The shear strength of bovine cortical bone was found to be 34 MPa (similar to the $\sim$ 35 MPa figure for thermally sprayed HAp coatings).

4. The shear strength of dual HAp coatings on Ti was $\sim$ 11 MPa and Ti6Al4V was $\sim$ 14 MPa (30–40% of the 34 MPa benchmark). This was because α-titanium < α-HAp, causing residual tensile stresses in the coating, thereby promoting cracking.

5. The shear strength of dual HAp coatings on 316L stainless steel was $\sim$ 22 MPa ($\sim$ 65% of the 34 MPa benchmark). This was because α-316L > α-HAp, causing residual compressive stresses in the coating, thereby promoting buckling, a less damaging effect than the tensile cracking caused by titanium substrates.

Acknowledgment

The authors gratefully acknowledge Mr D. Russell of the Graduate School of Biomedical Engineering workshop, University of New South Wales, for the fabrication of the testing rig.

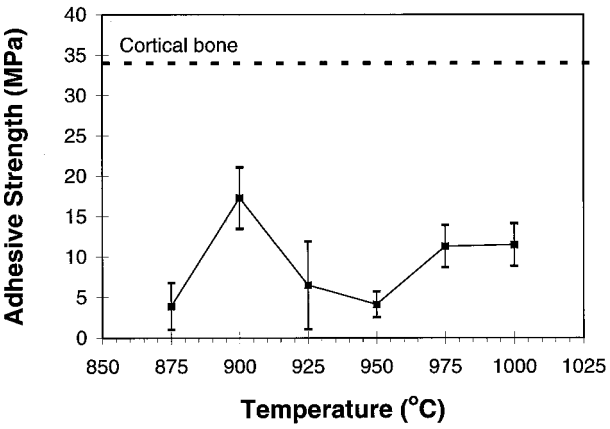

Figure 18 Interfacial shear strength, as a function of densification temperature, for a Ti6Al4V substrate.

References

1. C. C. BERNDT, G. N. HADDAD, A. J. D. FARMER and K. A. GROSS, *Mater. Forum* **14** (1990) 161.
2. J. C. KNOWLES, K. GROSS, C. C. BERNDT and W. BONFIELD, *Biomaterials* **17** (1996) 639.
3. P. DUCHEYNE, W. V. RAEMDONCK, J. C. HEUGHEBAERT and M. HEUGHEBAERT, *ibid.* **7** (1986) 97.
4. A. J. RUYS, K. A. ZEIGLER, B. K. MILTHORPE and C. C. SORRELL, in ''Ceramics: adding the value,'' edited by M. J. Bannister (CSIRO, Melbourne, 1992) p. 591.
5. A. J. RUYS, N. EHSANI, B. K. MILTHORPE and C. C. SORRELL, *J. Aust. Ceram. Soc.* **29** (1993) 65.
6. P. DUCHEYNE, S. RADIN, M. HEUGHEBAERT and J. C. HEUGHEBAERT, *Biomaterials* **11** (1990) 244.
7. A. J. RUYS, C. C. SORRELL, A. BRANDWOOD and B. K. MILTHORPE, *J. Mater. Sci. Lett.* **14** (1995) 744.
8. A. J. RUYS, A. BRANDWOOD, B. K. MILTHORPE, M. R. DICKSON, K. A. ZEIGLER and C. C. SORRELL, *J. Mater Sci: Mater. Med.* **6** (1995) 297.
9. M. WEI, A. J. RUYS, M. V. SWAIN, B. K. MILTHORPE and C. C. SORRELL, manuscript in preparation.
10. M. WEI, A. J. RUYS, B. K. MILTHORPE, A. BRANDWOOD and C. C. SORRELL, in Proceedings of the 2nd International Meeting of Pacific Rim Ceramic Societies, Cairns 1996, edited by P. A. Walls, C. C. Sorrell, and A. J. Ruys (Australasian Ceramic Society, Sydney) in press.
11. I. ZHITOMIRSKY and L. GAL-OR, *J. Mater. Sci: Mater. Med.* **8** (1997) 213.
12. M. JARCHO, C. H. BOLEN, M. B. THOMAS, J. BOBICK, J. F. KAY and R. H. DOREMUS, *J. Mater. Sci.* **11** (1976) 2027.
13. M. J. FILIAGGI and R. M. PILLIAR, *ibid.* **26** (1991) 5383.
14. M. D. DRORY and J. W. HUTCHINSON, *Proc. Royal Soc. Math. Phys. Eng. Sci.* **452** (1996) 2319.
15. ''Standard Test Methods for Adhesion of Metallic Coatings,'' ASTM Standard B571-91.
16. ''Standard Test Methods for Measuring Adhesion by Tape Test,'' ASTM Standard D3359-92.
17. ''Standard Test Method for Shear Strength of Adhesive Bonds between Rigid Substrates by the Block-Shear Method,'' ASTM Standard D4501-91.
18. ''Standard Test Method for Adhesion or Cohesive Strength of Flame-Sprayed Coating,'' ASTM Standard C633-79.
19. ''Standard Test Method for Tension of Porous Metal Coatings,'' ASTM Standard F1147-88.
20. ''Standard Test Methods for Shear Testing of Porous Metal Coatings,'' ASTM Standard F1044-87.

21. T. ARAI, H. FUJITA and M. WATANABE, *Thin Solid Films* **154** (1987) 387.
22. K. L. MITTAL, in ''Adhesion measurement of thin films, thick films, and bulk coatings,'' edited by K. L. Mittal (ASTM, Philadelphia, PA, 1976) p. 5.
23. M. V. SWAIN and J. MENCIK, *Thin Solid Films* **253** (1994) 204.
24. V. SAHAY, P. J. LARE and H. HAHN, in ''Characterisation and performance of calcium phosphate coatings for implants,'' edited by E. Horowitz and J. E. Parr (ASTM, Philadelphia, PA, 1994) p. 81.
25. A. J. D. FARMER, N. GANE and R. SEKEL, *Int. Ceram. Monogr.* **1** (1994) 94.

Received 20 April
and accepted 27 August 1998